Mechanical characterisation of nanocrystalline graphite using micromechanical structures

Mechanical characterisation of nanocrystalline graphite using micromechanical structures

S J Fishlock[a, b, c *], D Grech[b, d], J W McBride [a, c], H M H Chong [b], S H Pu [a, b, c]

[a] University of Southampton Malaysia Campus, Nusajaya 79200, Johor, Malaysia
[b] Nano Research Group, Electronics and Computer Science, University of Southampton, Southampton SO17 1BJ, UK
[c] Electromechanical Research Group, Faculty of Engineering and the Environment, University of Southampton, Southampton SO17 1BJ, UK
[d] National Centre for Advanced Tribology at Southampton (nCATS), University of Southampton, Southampton SO17 1BJ, UK

Conductive nanocrystalline graphite has been deposited using plasma-enhanced chemical vapour deposition at 750 °C, directly onto silicon substrates without any catalyst and fabricated into micromechanical membrane and beam structures. Using the buckling profile of the membrane and beam structures, we measure a built-in strain of -0.0142 and through wafer-bow measurement, a compressive stress of 436 MPa. From this we have calculated the Young's modulus of nanographite as 23.0 +/- 2.7 GPa. This represents a scalable method for fabricating nanographite MEMS and NEMS devices via a microfabrication-compatible process and provides useful mechanical properties to enable design of future devices.

1 Introduction

Graphene, thin-film graphite and graphene derivatives such as graphene-oxide (GO) are promising carbon based materials for micro and nano-electromechanical systems (MEMS/NEMS), and also as passive freestanding structures such as gas filtration membranes. The main properties of interest include good mechanical stiffness and strength [1] and electrical conductivity [2].

For example, graphene sheets and GO have been demonstrated as NEMS resonators [1,3,4] for high frequency sensors and signal processing applications; where the high stiffness and ultimate thinness are attractive for high sensitivity devices. GO is also of high interest for molecular filtration membranes [5,6] where molecules selectively pass through the defects in the crystal structure.

Currently the most widely used synthesis methods for large-scale graphene require a catalyst, for example copper or single-crystal germanium, and a subsequent transfer process onto the device substrate [7-9]. This is not cost-effective and can introduce defects such as wrinkling and polymer contamination. GO is typically synthesised through exfoliation of graphite-oxide [10], which then requires a transfer through manual adhesion, and typically when produced on a large-scale has thickness variations. This processing route represents a significant departure from standard microfabrication technologies.

Related materials such as amorphous tetrahedral-carbon and diamond-like carbon are readily deposited on a wafer-scale by methods including pulsed laser deposition and filtered cathodic vacuum arc [11-14]. Such films have had application particularly for devices where low friction is of interest [11, 12] however typically have relatively poor electrical conductivity and extremely high intrinsic stress (>1 GPa) which leads to poor substrate adhesion, this has limited their use somewhat within released and freestanding MEMS applications.

As an alternative carbon-based material, plasma-enhanced CVD (PECVD) using methane as a carbon precursor provides a scalable, microfabrication-compatible method to deposit nanocrystalline graphene (nanographene) and nanocrystalline graphite (nanographite) thin films directly onto insulating substrates such as silicon and silicon dioxide (SiO_2) [15-20] thereby removing the need for transferal of the film between substrates. Nanographite films typically have crystallites on the order of 10 nm, and a higher electrical resistivity compared with pristine graphene. Nanographite has been shown to have promising performance for transparent electrode applications [15, 16], as a strain sensor due to its high piezoresistive coefficient [17], in photovoltaics [18], in electronics [19], and as a potential material for MEMS/NEMS applications [20].

In this work, the fabrication of micromechanical structures and mechanical characterisation of PECVD nanographite is presented. The stress is extracted using wafer bow measurements and the Young's modulus of nanographite is then calculated using the buckling effect of both micromechanical membranes and doubly-clamped beams. These fundamental mechanical properties are essential for the future design of MEMS and NEMS using nanographite, and demonstrate a simple route for fabricating released structures. This represents a useful addition alongside the development of graphene, GO and other carbon materials, whereby some of the material properties are exchanged for the much greater ease of fabrication and integration afforded by catalyst-free PECVD.

2 Materials and methods

2.1 Film characterisation

Raman spectroscopy (Renishaw inVia) was used to characterise the structural properties of the nanographite film, using 532 nm wavelength excitation laser.

In order to image the material topology, a scanning electron micrograph of the film was taken using JEOL JSM FESEM 6700F at 80,000 times magnification. An atomic force microscope (Bruker Multimode AFM) in contact mode was used over a 1×1 μm scanning area to measure the film roughness.

The buckling amplitude of square nanographite membranes and beams were analysed using white-light interferometry (Polytec MSA-400). The thickness of each membrane was measured using ellipsometry (J. A. Woolham M2000), and side length was measured using optical microscopy. The stress of the nanographite film was determined using the wafer bow technique, a commercial measurement tool (KLA FLX) was used for bow measurement.

The electrical conductivity of the film was measured using micro-machined 'transmission-line model' structures [21], with nickel/titanium electrodes of increasing separation (20 to 100 μm separation) deposited onto an electrically isolated mesa of the nanographite film. I-V characteristics were obtained using a 'Cascade Microtech' probe station and 'Agilent B1500A Semiconductor' network analyser. A voltage sweep between - 10 and 10 V was applied.

2.2 Micromechanical device fabrication

A commercial PECVD tool (Oxford Instruments Nanofab1000 Agile) was used to deposit nanographite onto 6-inch silicon wafers. The deposition conditions are summarised in table 1. The hydrogen acts as a diluent, controlling deposition rate and promoting graphitic carbon growth by etching amorphous carbon [16]. The relatively high deposition temperature of 750 was used, since this was the minimum temperature to obtain graphitic carbon growth, below which amorphous carbon or no deposition occurs. Similar PECVD films have growth temperatures ranging from 525-900°C [16,19]. A deposition rate of approximately 2 nm per minute was measured, and the average final thickness of the film was measured across the wafer using white-light ellipsometry.

Temperature	750 °C
Chamber pressure	1500 mTorr
H_2 flow	75 sccm
CH_4 flow	60 sccm
RF Power	100 W

Table 1. Summary of deposition conditions

Figure 1 shows the main fabrication steps of separate membrane and doubly-clamped beam microstructures. Silicon wafers were first RCA cleaned and then a 400 nm thin film of SiO_2 was deposited by PECVD using an Oxford Instruments system 100. For the membranes, 280 nm of nanographite was deposited onto the SiO_2 layer (figure 1-A). 1.5 μm SiO_2 was then deposited using PECVD onto both back and frontside, and squares were patterned onto the backside SiO_2 and etched using Ar/CHF_3 reactive ion etching (RIE) (figure 1-B). The silicon handle was then etched using tetramethylammonium hydroxide (TMAH) leaving 30 μm of silicon. Complete silicon etching was

achieved using Ar/SF_6 inductively-coupled plasma (ICP) etch until the buried SiO2 film [22]. The buried and front-side SiO_2 layers were then etched using RIE, fully releasing the nanographite membrane with side lengths between 190 and 275 µm (figure 1-C). An optical microscope image of a membrane is shown in figure 2-A.

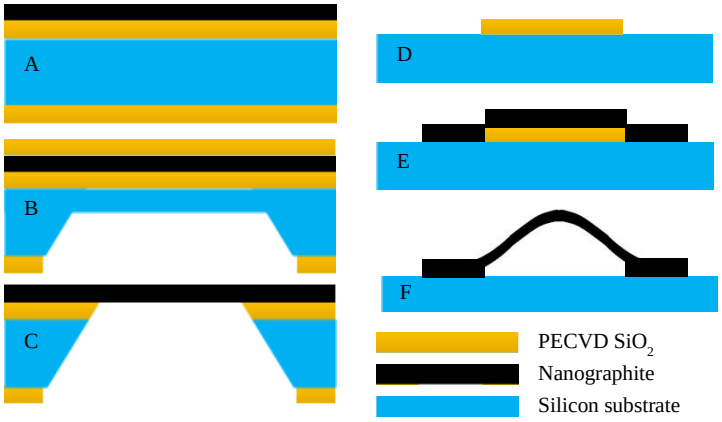

Figure 1. Fabrication flow schematic for nanographite membrane (A-C) and doubly-clamped beam (D-F).

For the beams, a 200 nm thick SiO_2 film was deposited using PECVD and patterned using photolithography and RIE. This creates a sacrificial spacer defining the released beam length (figure 1-D). Subsequently, 400 nm of nanographite was deposited over the spacer, and patterned into a beam with large anchors (figure 1-E). The nanographite is etched using O_2-based RIE. HF vapour, with the sample heated at 40 °C, is then used to isotropically etch the SiO_2 spacer and release the beam (figure 1-F). Beam lengths between 65 and 140 µm have been fabricated. A scanning electron micrograph of a buckled beam shown is in figure 2-B.

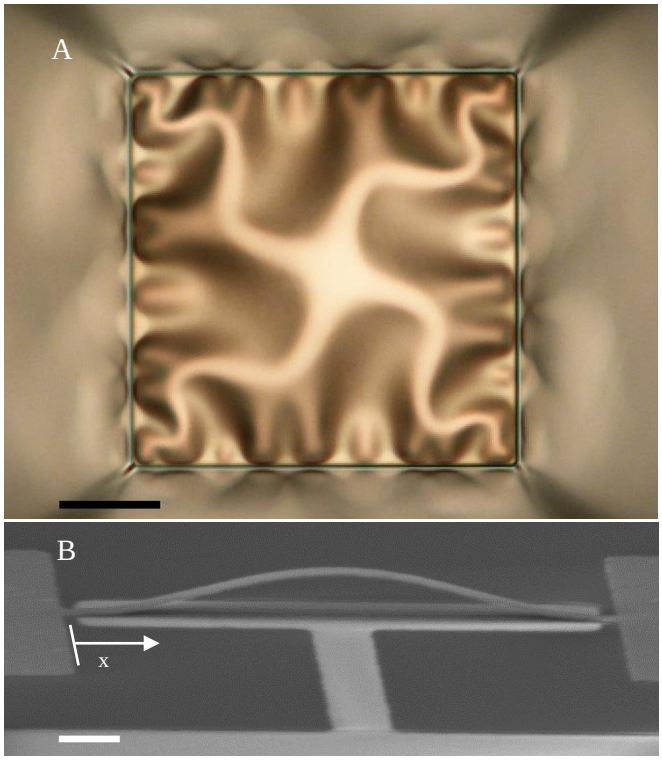

Figure 2. (A) Optical microscope image of 193.3 μm nanographite membrane, view taken from backside. (B) SEM image of fabricated 140.0 μm nanographite beam, taken at high 80° angle. Scale bar (A) 50 μm (B) 20 μm.

3 Theory/calculation

3.1 Membrane buckling

The buckling behaviour of square micromechanical membranes has been utilised as a method to characterise the Young's modulus of, for example, Si_3N_4 membranes [23.24]. Here, the buckling characterisation of membranes will be applied to nanographite membranes, such as shown in figure 2-A, for the calculation of the material Young's modulus.

The geometry of compressively stressed square membranes has been shown to lie within 3 regimes, defined by their buckling shape, depending on the level of in-plane strain. For regime 1, $\sigma < \sigma_{crit1}$ and the membrane is flat. In regime 2, when $\sigma_{crit1} < \sigma < \sigma_{crit2}$, the membrane is buckled with rotational and four-fold symmetry. In regime 3, $\sigma > \sigma_{crit2}$ and the membrane is buckled with rotational symmetry only. Mathematical analysis using energy-minimisation techniques of the buckling behaviour of square membranes has been undertaken previously by Ziebart *et al.* [23]. This analysis establishes a relation between the maximum out-of-plane amplitude of a buckled square membrane, and the in-plane strain of the material. The analysis uses dimensionless displacements where the pre-strain $\bar{\varepsilon}_0$ is given in equation 1, in terms of the strain ε, side length a, and thickness h:

$$\bar{\varepsilon}_0 = \frac{\varepsilon \cdot a^2}{h^2} \quad (1)$$

The dimensionless deflection $\bar{w}$ is defined in terms of the real maximum deflection *w*

$$\bar{w} = \frac{w}{h} \quad (2)$$

and a fitted displacement function $\bar{w}_{0\,fit}$ extracted from energy minimisation is given by

$$\bar{w}_{0\,fit} = \sqrt{\Delta\bar{\varepsilon}_0 (c_1 + c_2 \tanh\left\{c_3 \Delta\bar{\varepsilon}_0\right\} + \frac{\left\{c_4 \Delta\bar{\varepsilon}_0 + c_5 \Delta\bar{\varepsilon}_0^{\,2}\right\}}{1 - c_6 \Delta\bar{\varepsilon}_0^{\,3}}} \quad (3)$$

where the fitting parameters $c_1 - c_6$ are calculated as in equation 4, where *v* is the Poisson's ratio.

$$\begin{pmatrix} c_1 \\ c_2 \\ c_3 \\ c_4 \\ c_5 \\ c_6 \end{pmatrix} = \begin{pmatrix} -0.4972 & -0.2314 & -0.2128 \\ 0.0698 & 0.1625 & 0.200 \\ -7.19\times10^{-3} & -0.0466 & 0.0367 \\ -1.19\times10^{-3} & 0 & 5.51\times10^{-3} \\ -3.34\times10^{-6} & -7.43\times10^{-5} & 1.28\times10^{-4} \\ 3.16\times10^{-6} & 4.80\times10^{-6} & -1.52\times10^{-5} \end{pmatrix} \bullet \begin{pmatrix} 1 \\ \nu \\ \nu^2 \end{pmatrix} \quad (4)$$

3.2 Stress measurement

The stress has been separately calculated by measuring the change in the level of bowing from the substrate before and after the deposition of the nanographite film, using the commonly used Stoney's equation (5), where σ is the film stress, E_S is the biaxial Young's modulus of the substrate, v_s is the substrate Poisson's ratio, t_s and t_f are the thickness of substrate and film respectively, and R_0 and R are the radius of curvature before and after film deposition.

$$\sigma = \frac{E_s}{6(1-\nu_s)} \frac{t_s^{\,2}}{t_f} \left(\frac{1}{R} - \frac{1}{R_0} \right) \quad (5)$$

From the measured values of stress and strain, ε, the Young's modulus *E* can be extracted from the following relationship (6) [23].

$$E = \frac{(1-\nu)\sigma}{\varepsilon} \quad (6)$$

3.3 Beam buckling

To provide a second, independent measurement of the Young's modulus of the nanographite film, the buckling behaviour of doubly-clamped beams has been used. Analytical solution for the amplitude of a doubly-clamped beam is presented by Nayfeh *et al.* [25]. The beam follows the mode shape as described in (7), where the amplitude *w* along the length *x* (figure 2-B) is given by:

$$w(x) = c\left[1 - \cos\left(2\pi x\right)\right] \qquad (7)$$

$$\text{where } c = \pm 2\sqrt{\frac{Pl^2}{EI\lambda^2} - 1} \text{ and } w = \frac{\hat{w}}{\sqrt{I/A}} \quad (8)$$

Where the in-plane force is P, second moment of area I and cross-sectional area of the beam is A, λ is an eigenvalue corresponding to the mode shape and $\hat{w}$ is the out of plane buckling amplitude. Since the beam is of a high width to thickness ratio $w/h > 5$, it is under plane strain condition and E is replaced by effective Young's modulus $\widehat{E} = E(1-\nu^2)$ [26].

The doubly-clamped beams were then modeled using commercial finite element (FE) analysis software ANSYS to verify the analytical results, with biaxial strain applied to the beam. Non-linear static analysis was undertaken, with the maximum buckled amplitude measured. Whereas the analytical solution is based on an idealised beam model, with two fully clamped beam ends, the release process creates steps or kinks in the beam equal to the thickness of the sacrificial SiO_2. The simulations account for these anchors as shown in figure 5-A.

4 Results

4.1 Film characterisation

The measured Raman spectrum of nanographite is shown in figure 3 with the main features denoted. The presence of the G (1593 cm^{-1}) peak shows sp^2 bonded carbon, and the D peak arises from defects within the graphite lattice, such as grain boundaries. The ratio of intensities of the two peaks I_D/I_G confirms a nanocrystalline grain structure [27] and the location of the G peak is a strong indicator of the magnitude of the stress of graphitic films [28]. The G peak for graphitic materials under zero applied stress is located at around 1579 cm^{-1}, whilst the G peak in this nanographite film is at 1593 cm^{-1}. This red-shift of the peak demonstrates a significant compressive stress in the film. This is caused by a combination of thermal stress due to the mismatch in thermal expansion coefficients between the nanographite and silicon substrate, and other intrinsic stress effects from the deposition. This is consistent with other PECVD films such as Si_3N_4 which are typically in a state of high residual stress [29, 30].

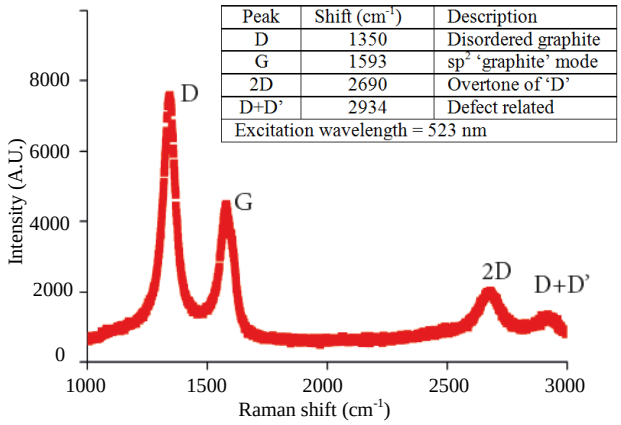

Figure 3. Raman spectrum of nanographite with main peaks denoted.

A scanning electron micrograph showing the topology of the film is shown in figure 4. This shows the film to comprise of nano-graphitic crystallites and this topology and grain structure show good agreement with similar films [15-19]. From AFM measurements the film has an RMS roughness of 2.58 nm, Conductivity of the film has been measured using transmission-line measurements as 99.7 S cm^{-1}.

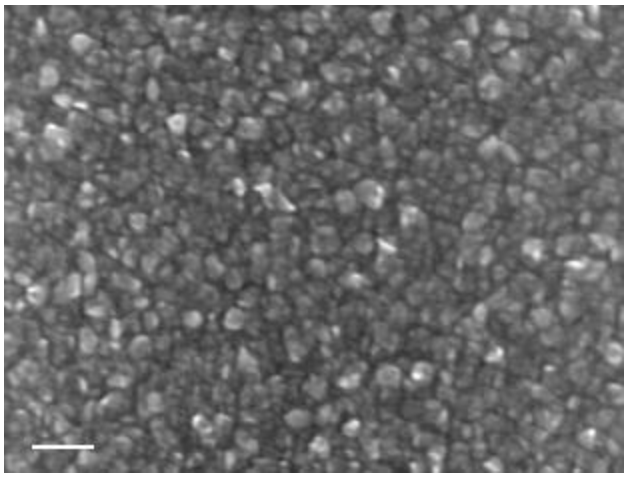

Figure 4. SEM image of film morphology. Inset scale bar is 100 nm.

4.2 Mechanical characterisation of membrane devices

The Young's modulus of the nanographite film has been calculated initially using the buckling behaviour of square membranes, by fitting the results for the maximum buckled amplitude of membranes into equation 2, section 3.1, to the experimentally measured characteristics of nanographite membranes. The in-plane strain is compressive, with the results detailed in table 2 showing the average as-deposited strain to be -0.0142, where negative denotes compressive strain, assuming $\nu = 0.25$. The constants required to calculate the strain in equation 4 show a weak

dependency on the Poisson's ratio ν, which has not been measured. In this case, an estimate is made for ν to lie between 0.16, of well-ordered graphite, [31] and 0.31, of isotropic graphite [32]. All fabricated membranes lie within regime buckling 3 as summarised in section 3.1.

Side length (μm)	Maximum Deflection (μm)	Thickness (nm)	Strain
221.0	16.6	281	-0.013
193.3	15.3	281	-0.014
273.4	24.0	285	-0.017
224.9	19.2	285	-0.016
217.4	15.8	275	-0.012
192.6	14.9	296	-0.013
		Average	-0.014

Table 2. Summary of membrane geometry and strain calculation.

Using equation 5, the residual stress of the nanographite film is determined as 436 MPa compressive. The stress is the same (within the accuracy of the wafer bow measurement tool) for the deposition of membranes and beams. Using equation 6, and after taking into account measurement errors for stress, membrane geometry and the possible range of Poisson's ratio (0.16-0.31), the extracted Young's modulus value is 23.0 +/- 2.7 GPa.

4.3 Mechanical characterisation of beam devices

Analytical and FE simulation of the buckled nanographite beams has been performed to further verify the value of E obtained from the membrane structures. The maximum buckling amplitude of doubly-clamped beams is calculated analytically using equation 7, assuming the value E = 23 GPa as calculated using the membrane buckling behaviour. This result is then compared with the buckling amplitude of actual beams as measured experimentally through white-light interferometry. FE analysis, more closely representing the actual as-fabricated beam geometry, shows a closer agreement between the fabricated structures, with 1.2 % underestimation between simulation and experimental results. Figure 5 shows a simulation result of a buckled beam with non-ideal anchors highlighted.

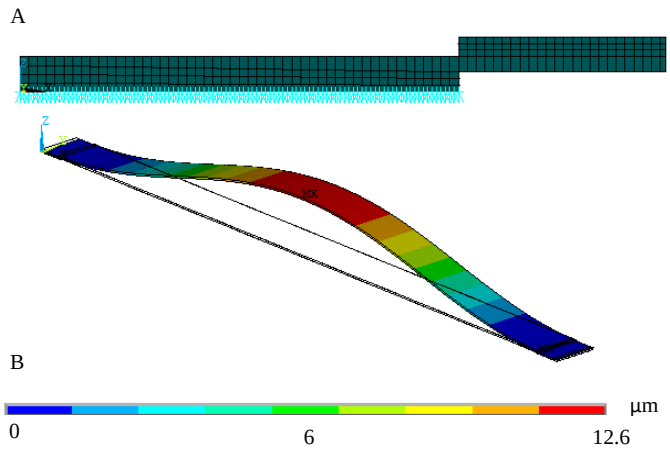

Figure 5. (A), anchor clamping condition, and (B) simulation result of 140 µm buckled beam showing out of plane deflection.

A comparison of buckling amplitude between simulation, analytical and measured results is shown in table 3. The relative difference between the measured results is shown in brackets, indicating a good agreement between simulation and measured results.

Beam length (µm)	Thickness (nm)	Amplitude measured (µm)	Amplitude, FE (µm)	Amplitude, analytical (µm)
65.0	409	7.0	6.1 (-13.4%)	5.1 (-27.1%)
90.0	398	8.5	8.3 (-2.8%)	7.0 (-17.6%)
140.0	394	12.8	12.6 (-1.2%)	11.0 (-14.1%)

Table 3. Summary of beam buckling amplitude measurements.

5 Discussion

The measured Young's modulus value for nanographite of 23 GPa is relatively low compared with pristine graphite or graphene and other carbon forms such as diamond-like carbon (~300 GPa) [11]. This is the intrinsic material Young's modulus, which, in a freestanding structure, can be effectively altered by application of stress. The stiffness of polycrystalline graphite is strongly dependent on the orientation of its grains, and the misalignment between grains parallel to the substrate causes a low in-plane stiffness [33].

For the buckling behaviour of the doubly clamped beams, both FE and analytical models show a trend of increasing agreement to the measured result at the longest beam lengths (140 μm). The FE results show a small 1.2 % under-estimation of the buckled amplitude for the longest beams, compared with a 13.4 % underestimation for the shortest. This can be explained by an increased level of compliance in the beam anchors, as modelled by Kobrinsky *et al* [34], which is less dominant for longer beams. Nevertheless, the FE result agrees well with the measured result for longer beams, which confirms that the extracted *E* value is reliable.

We note that the relatively high stress, though lower than in DLC films, and low modulus of the nanographite material are not of interest for some MEMS applications. For certain applications such as bi-stable switches and memory devices, [35,36] where the mechanical non-linearity brought about by buckling, and a low pull-in voltage are sought after; and also for graphitic gas-separation membranes, the material is of significant interest. The measured mechanical properties obtained in this work are useful for the future design of such devices. Furthermore, the tuning of PECVD parameters could lead to the deposition of larger-grained graphitic material, which, since the mechanical properties of graphites are very highly orientation-dependent, could realise a significant increase in both the *E* and lowering stress state of the film.

6 Conclusions

In summary, mechanical characterisation of nanographite, deposited directly onto silicon substrates using PECVD, has been demonstrated using micromechanical membranes and doubly-clamped beams. An average compressive residual stress of 436 MPa and a compressive pre-strain of -0.0142 has been measured, and from this, a Young's modulus value of 23.0 +/- 2.7 GPa was determined.

7 Acknowledgements

We gratefully acknowledge fabrication assistance from the Southampton Nanofabrication Centre. The financial assistance from the Faculty of Engineering and the Environment at the University of Southampton, and the Malaysian Ministry of Education under grant FRGS/2/2014/TK03/USMC/02/1 is also acknowledged. We thank Dr Sean O'Shea for guidance and Mr Andrew Breeson (both IMRE, A-STAR) for useful assistance using SEM.

8 References

[1] J.S. Bunch, A.M. van der Zande, S.S. Verbridge, I.W. Frank, D.M. Tanenbaum, J.M. Parpia, H.G. Craighead, P.L. McEuen, Electromechanical resonators from graphene sheets., Science. 315 (2007) 490–3.

[2] S. Stankovich, D. a. Dikin, R.D. Piner, K. a. Kohlhaas, A. Kleinhammes, Y. Jia, S T. Nguyen, R. S. Ruoff, Synthesis of graphene-based nanosheets via chemical reduction of exfoliated graphite oxide, Carbon. 45 (2007) 1558–1565.

[3] A.M. van der Zande, R. a Barton, J.S. Alden, C.S. Ruiz-Vargas, W.S. Whitney, P.H.Q. Pham, J. Park, J.M. Parpia, H.G. Craighead, P.L. McEuen, Large-scale arrays of single-layer graphene resonators., Nano Lett. 10 (2010) 4869–73.

[4] Robinson, J. T., Zalalutdinov, M., Baldwin, J. W., Snow, E. S., Wei, Z., Sheehan, P., Houston, B. H. (2008). Wafer-scale reduced graphene oxide films for nanomechanical devices. *Nano Letters*, *8*(10), 3441–5.

[5] H. Li, Z. Song, X. Zhang, Y. Huang, S. Li, Y. Mao, H. J. Ploehn, Y. Bao, M. Yu, Ultrathin, Molecular-Sieving Graphene Oxide Membranes for Selective Hydrogen Separation, Science (80). 342 (2013) 95–98.

[6] H.W. Kim, H.W. Yoon, S. Yoon, B.M. Yoo, B.K. Ahn, Y.H. Cho, H. J. Shin, H. Yang, U. Paik, S. Kwon, Selective Gas Transport Through few-layered graphene and graphene oxide membranes, Science (80). 342 (2013) 91–95.

[7] S. Bae, H. Kim, Y. Lee, X. Xu, J. Park J.S. Park, Y. Zheng, J. Balakrishnan, T. Lei, H. R. Kim, Y. I. Song, Y.J. Kim, K. S Kim, B. Ozyilmaz, J.H. Ahn, B. H. Hong, S. Iijima, Roll-to-roll production of 30-inch graphene films for transparent electrodes, Nat. Nanotechnol. 5 (2010) 1–5.

[8] L. Gao, G.-X. Ni, Y. Liu, B. Liu, A.H. Castro Neto, K.P. Loh, Face-to-face transfer of wafer-scale graphene films., Nature. 505 (2014) 190–4.

[9] J. Lee, E. Lee, W. Joo, Y. Jang, B. Kim, Wafer-scale growth of single-crystal monolayer graphene on reusable hydrogen-terminated germanium, Science (80). 344 (2014) 286–289.

[10] G. Eda, G. Fanchini, M. Chhowalla, Large-area ultrathin films of reduced graphene oxide as a transparent and flexible electronic material, Nat. Nanotechnol. 3 (2008) 270–274.

[11] J.K. Luo, Y.Q. Fu, H.R. Le, J. a Williams, S.M. Spearing, W.I. Milne, Diamond and diamond-like carbon MEMS, J. Micromechanics Microengineering. 17 (2007) S147–S163.

[12] B.. Tay, D. Sheeja, L.. Yu, On stress reduction of tetrahedral amorphous carbon films for moving mechanical assemblies, Diam. Relat. Mater. 12 (2003) 185–194.

13] M. Tomi, A. Isacsson, M. Oksanen, D. Lyashenko, J.-P. Kaikkonen, S. Tervakangas, J. Kolehmainen, P. J. Hakonen, Buckled diamond-like carbon nanomechanical resonators, Nanoscale. 7 (2015) 14747–14751.

[1] a. C. Ferrari, B. Kleinsorge, N. a. Morrison, a. Hart, V. Stolojan, J. Robertson, Stress reduction and bond stability during thermal annealing of tetrahedral amorphous carbon, J. Appl. Phys. 85 (1999) 7191-7197.

[15] H. Medina, Y. Lin, C. Jin, C. Lu, C. Yeh, K. Huang, K. Suenaga, J. Robertson, P. Chiu, Metal-Free Growth of Nanographene on Silicon Oxides for Transparent Conducting Applications, Adv. Funct. Mater. 22 (2012) 2123–2128.

[16] L. Zhang, Z. Shi, Y. Wang, R. Yang, D. Shi, G. Zhang, Catalyst-free growth of nanographene films on various substrates, Nano Res. 4 (2010) 315–321.

[17] J. Zhao, C. He, R. Yang, Z. Shi, M. Cheng, W. Yang, Dongxia S, Guangyu Z, Ultra-sensitive strain sensors based on piezoresistive nanographene films, Appl. Phys. Lett. 101 (2012) 063112.

[18] G. Kalita, M.S. Kayastha, H. Uchida, K. Wakita, M. Umeno, Direct growth of nanographene films by surface wave plasma chemical vapor deposition and their application in photovoltaic devices, RSC Adv. 2 (2012) 3225–3230.

[19] M.E. Schmidt, C. Xu, M. Cooke, H. Mizuta, H.M.H. Chong, Metal-free plasma-enhanced chemical vapor deposition of large area nanocrystalline graphene, Mater. Res. Express. 1 (2014) 025031.

[20] N. Lindvall, J. Sun, G. Abdul, A. Yurgens, Towards transfer-free fabrication of graphene NEMS grown by chemical vapour deposition, Micro Nano Lett. 7 (2012) 3–6.

[21] D. K. Schroder, Semiconductor Material and Device Characterisaiton, John Wiley and Sons, New York, USA (2006).

[22] D. Grech, K.S. Kiang, J. Zekonyte, M. Stolz, R.J.K. Wood, H.M.H. Chong, Highly linear and large spring deflection characteristics of a Quasi-Concertina MEMS device, Microelectron. Eng. 119 (2014) 75–78.

[23] V. Ziebart, O. Paul, H. Baltes, Strongly buckled square micromachined membranes, J. Microelectromechanical Syst. 8 (1999) 423–432.

[24] T. Kramer, O. Paul, Postbuckled micromachined square membranes under differential pressure, J. Micromechanics Microengineering. 12 (2002) 475–478.

[25] A.H. Nayfeh, S. a. Emam, Exact solution and stability of postbuckling configurations of beams, Nonlinear Dyn. 54 (2008) 395–408.

[26] P.M. Osterberg, S.D. Senturia, M-test: A Test Chip For Mems Material Property Measurement Using Electrostatically Actuated Test Structures, J. Microelectromechanical Syst. 6 (1997) 286–286.

[27] L. Cancado, K. Takai, T. Enoki, General equation for the determination of the crystallite size L a of nanographite by Raman spectroscopy, Appl. Phys. Lett. 88 (2006) 163106 1-3.

[28] M. Hanfland, H. Beister, K. Syassen, Graphite under pressure: Equation of state an first-order Raman modes, Phys. Review B. 39 (1989) 598-603.

[29] H. Huang, K.J. Winchester, a. Suvorova, B.R. Lawn, Y. Liu, X.Z. Hu, J. M. Dell, L. Faraone, Effect of deposition conditions on mechanical properties of low-temperature PECVD silicon nitride films, Mater. Sci. Eng. A. 435-436 (2006) 453–459.

[30] E. Cianci, a. Schina, a. Minotti, S. Quaresima, V. Foglietti, Dual frequency PECVD silicon nitride for fabrication of CMUTs' membranes, Sensors Actuators A Phys. 127 (2006) 80–87.

[31] O.L. Blakslee, D.G. Proctor, E.J. Seldin, G.B. Spence, T. Weng, Elastic constants of compression-annealed pyrolytic graphite, J. Appl. Phys. 41 (1970) 3373.

[32] J.B. Spicer, F.W. Zeng, K. Han, Effects of Graphite Porosity and Anisotropy on Measurements of Elastic Modulus using Laser Ultrasonics, (2014) 232–235.

[33] B. T. Kelly, Physics of Graphite, Applied Science Publishers. (1981).

[34] M.J. Kobrinsky, E.R. Deutsch, S.D. Senturia, Effect of support compliance and residual stress on the shape of doubly supported surface-micromachined beams, J. Microelectromechanical Syst. 9 (2000) 361–369.

[35] B. Charlot, W. Sun, K. Yamashita, H. Fujita, H. Toshiyoshi, Bistable nanowire for micromechanical memory, J. Micromechanics Microengineering. 18 (2008) 045005.

[36] Y. Tsuchiya, K. Takai, N. Momo, T. Nagami, S. Yamaguchi, T. Shimada, et al., Nanoelectromechanical nonvolatile memory device incorporating nanocrystalline Si dots, J. Appl. Phys. 100 (2006) 094306.